Fig. 9. Unnamed pre-Tolstojan crater (−21°, 28°; 110 km diameter). Crater is almost completely obliterated; only the rim crest is partly preserved. Intercrater plains overlie the rim (FDS 27428). (North at top.)

of craters from C_5 as the freshest to C_1 as the most degraded (see footnote in Sec. II.A). Examples were given for each of these classes for two sizes of crater, one between 20 and 100 km in diameter and the other larger than 100 km. Typical examples of Mercurian crater-degradational types are shown in Figs. 5–9.

This scheme was used extensively by geological mappers of the 1:5,000,000 scale quadrangles, and the system has proved useful in correlating ages in areas distant from suitable major impact basins. However, some difficulties have been encountered. For example, in the Shakespeare quadrangle (Guest and Greeley 1983), it was considered better to restrict Class 5 craters to those with dark or light halos, and/or rays. It was found that by including those craters that were fresh appearing but without rays within Class 5, virtually no Class 4 craters remained. As a result, the 150 km diameter crater Verdi was mapped as a C_4 crater despite its being the type example of Trask for a C_5 class of crater. It was recognized, however, that albedo patterns are less easy to distinguish close to the terminator, and crater form less easy to distinguish towards the limb. In consequence, no scheme can be applied with rigorous consistency until all of Mercury is imaged at different lighting angles.

A similar problem was encountered by Spudis and Prosser (1984) during the mapping of the Michelangelo quadrangle. They found that Dostoevskij (see Sec. II.B and Fig. 3) possessed a crater density indicating that it is one of the oldest basins on the planet. In contrast, Dostoevskij is the type example of a large C_3 (middle-age) crater in the Trask system (McCauley et al. 1981). Spudis and Prosser (1984) suggested that the stratigraphic significance of crater degradation is only approximate and that a variety of evidence, including regional geologic setting, proximity to other units, crater density, and type of postcrater modification, must be used in concert to establish the relative ages of Mercurian features.

III. STRATIGRAPHY

In the earliest stages of planetary geologic mapping, the first steps usually taken are terrain reconnaissance and classification. Later, when the relations between photogeologically defined units become clearer, it is desirable to establish a formal chronostratigraphic (i.e., time-stratigraphic) classification scheme in order to correlate widely-separated geologic units and provide a framework for interplanetary correlations of geologic time. Shoemaker and Hackman (1962) presented a chronostratigraphic classification for the Moon in which chronostratigraphic systems were defined on the basis of superposition relations of observable rock-stratigraphic units (Wilhelms 1970,1987*a*). This method, although modified by more detailed knowledge of lunar geology, is still in use today (Wilhelms 1987*a*).

The geology of Mercury was initially mapped with physiographic/terrain units, although an attempt was made to indicate their lithology and relative stratigraphic order (Trask and Guest 1975). Geologic mapping for the 1:5,000,000 scale quadrangle maps of the Mercurian hemisphere imaged by Mariner 10 relies on an informal rock-stratigraphic classification of crater, basin and plains units arranged in order of relative age (Holt 1978). After mapping was begun, McCauley et al. (1981) proposed a series of formal rock-stratigraphic units associated with the Caloris basin as the first step in formulating a stratigraphy for Mercury. Spudis (1985) described the use of the Caloris group of McCauley et al. (1981), together with newly defined rock-stratigraphic units, to develop a formal Mercurian chronostratigraphy (Table I).

The chronostratigraphic scheme developed for Mercury is very similar to the system used for the Moon. In Table I, the approximate ages of, and lunar equivalents to, the Mercurian systems are given, although exact correlations of the systems and times are not intended. This aspect of the history of Mercury is discussed below in Sec. IV.B.

A. pre-Tolstojan System

The two oldest Mercurian chronostratigraphic systems are divided by the deposits of the Tolstoj basin (see Sec. II.B). The informal pre-Tolstojan sys-

TABLE I
Mercurian Chronostratigraphic Scheme

System	Major Units	Approx. Age of Base of System[a]	Lunar Counterpart[b]
Kuiperian	crater materials	1.0 Gyr	Copernican
Mansurian	crater materials	3.0–3.5 Gyr	Eratosthenian
Calorian	Caloris Group; plains, crater, small-basin materials	3.9 Gyr	Imbrian
Tolstojan	Goya Formation; crater, small-basin, plains materials	3.9–4.0 Gyr	Nectarian
pre-Tolstojan	Intercrater plains, multiring basin, crater materials	pre–4.0 Gyr	pre-Nectarian

[a]Approximate ages based on the assumption of a lunar-type impact flux history on Mercury.
[b]Included for reference only; no implication of exact time correlation is intended.

tem includes all deposits formed before the impact that created the Tolstoj basin. The oldest recognizable pre-Tolstojan units are the remnants of ancient multiring basins (Fig. 2). The currently recognized population of pre-Tolstojan multiring basins is listed in Table II (designated pT). These basins are randomly distributed over the Mercurian surface (Fig. 10) and probably represent the remnants of a lunar-like, heavily cratered terrain. Some basin sites have served as depositional environments for later smooth plains units (see also Leake 1982), and many ring remnants are recognized by the deflection of later tectonic features into circular or arcuate patterns. Thus, this population of pre-Tolstojan basins forms the broad-scale structural framework for the subsequent geologic evolution of Mercury's surface.

Because of the degraded nature of these ancient basins, both the ring diameters and the original basin configuration are difficult to ascertain. However, in all of the basins, at least one ring appears to have more topographic or structural expression than others. These conspicuous rings are italicized in Table II and are considered to be the rings that were originally the basin rims, i.e., the structural equivalents of the main massif ring of Caloris (1340 km in diameter) or the Cordillera ring of the lunar Orientale basin. Diameters of the main rim are used in the crater-frequency curve of Fig. 11. This curve shows two parallel production functions. For the lower-size ranges, representative cratered terrain in the H-12 quadrangle was used. The crater curve at the larger diameters shows a distinct "knee" at about 500 km (Fig. 11). At diameters larger than 500 km, the function is again in production. These relations suggest that the population of large ancient basins represents only the large members of a heavily cratered surface, of which most craters smaller than about 500 km were obliterated.

TABLE II
Mercurian Multiring Basins

Basin[a]	Center	Age[b]	Ring Diameters (km)[c]	Comments[d]
CALORIS	30°,195°	C	(630),900,*1340*,(2050),(2700),(3700)	
TOLSTOJ	−16°,164°	T	(260),330,*510*,(720)	
VAN EYCK	44°,159°	T	150,285,(450),520	
SHAKESPEARE	49°,151°	pT	(200),*420*,680	
SOBKOU	34°,132°	pT	490,*850*,1420	Partly mapped by Croft (1979)
BRAHAMS-ZOLA	59°,172°	pT	340,*620*,840,(1080)	
HIROSHIGE-MAHLER	−16°,23°	pT	150,355,(700)	Partly mapped by Leake (1982)
MENA-THEOPHANES	−1°,129°	pT	260,475,*770*,1200	Partly mapped by Schaber et al. (1977)
TIR	6°,168°	pT	380,660,950,*1250*	
ANDAL-COLERIDGE	−43°,49°	pT	(420),700,1030,*1300*,1750	
MATISSE-REPIN	−24°,75°	pT	410,*850*,1250,(1550),(1990)	Partly mapped by Croft (1979)
VINCENTE-YAKOVLEV	−52°,162°	pT	360,725,950,1250,(1700)	Spudis and Prosser (1984)
EITOKU-MILTON	−23°,171°	pT	280,590,850,*1180*	Spudis and Prosser (1984)
Borealis	73°,53°	pT	860,*1530*,(2230)	Partly mapped by Trask and Strom (1976)
Derzhavin-Sor Juana	51°,27°	pT	*560*,740,890	Partly mapped by Schaber et al. (1977)
Budh	17°,151°	pT	580,*850*,1140	
Ibsen-Petrarch	−31°,30°	pT	425,*640*,930,1175	
Hawthorne-Riemenschneider	−56°,105°	pT	270,*500*,780,1050	Spudis and Prosser (1984)
(Gluck-Holbein)	35°,19°	pT	240,*500*,950	
(Chong-Gauguin)	57°,106°	pT	220,350,580,*940*	
(Donne-Moliere)	4°,10°	pT	375,700,(825),*1060*,1500	
(Bartok-Ives)	−33°,115°	pT	480,790,*1175*,(1500)	Spudis and Prosser (1984)
(Sadi-Scopas)	−82°5,44°	pT	360,600,*930*,(1310)	

[a]Basin names in capital letters definitely exist, names in upper-and-lowercase probably exist and names in parentheses possibly exist. Double names are applied to degraded, nearly obliterated basins following the practice devised for naming degraded basins on the Moon (Wilhelms and El-Baz 1977; Wilhelms 1987*a*).
[b]Relative age; C for Calorian; T for Tolstojan; pT for pre-Tolstojan.
[c]Italicized diameters correspond to physiographically most prominent ring (basin rim); diameters in parentheses reflect uncertain measurement due to discontinuous rings.
[d]References to previous studies that originally recognized degraded basins.

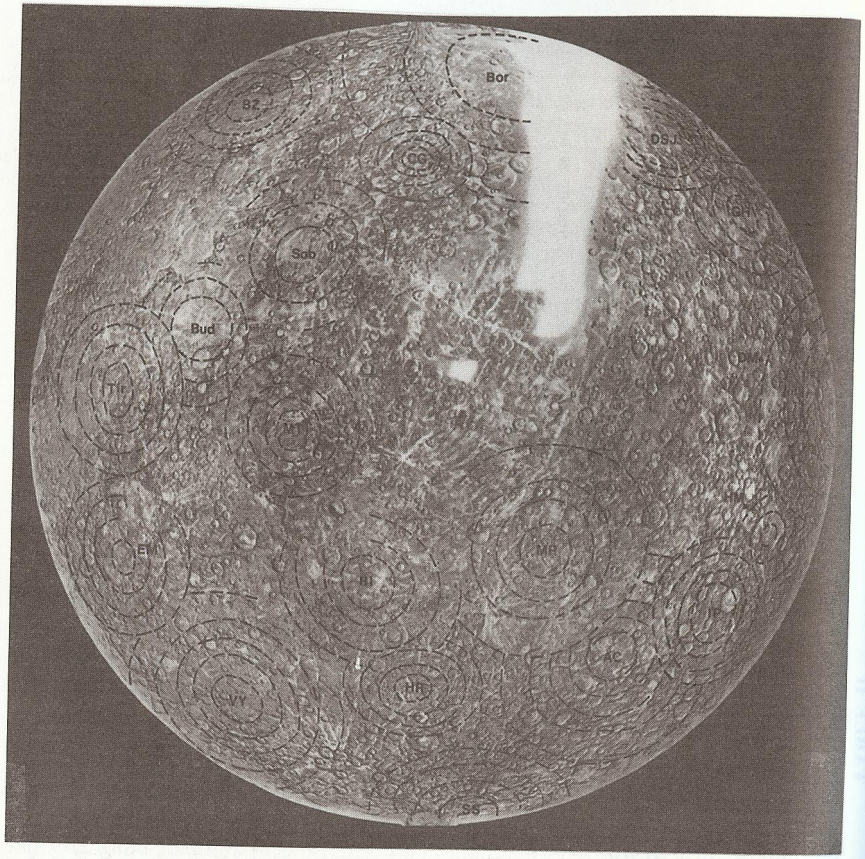

Fig. 10. Map showing the distribution of pre-Tolstojan basin rings. All basins shown here underlie the intercrater plains. Basins are listed in Table II. Base is Lambert Equal-Area projection, centered on 0°, 100°, showing hemisphere of Mercury imaged by Mariner 10. (North at top.)

Apparently, this ancient cratered surface on Mercury was largely erased by the widespread intercrater plains materials (Fig. 12). Trask and Guest (1975) considered that the intercrater plains represent an ancient primordial surface, mainly because so many secondary craters are superposed on the intercrater plains. Malin (1976*a*) observed that, in several regions, large craters can be detected underneath intercrater plains. Strom (1977) noted that the production of similar, although less extensive, highland plains on the Moon had likewise obliterated the smaller-crater populations in these regions. Noting the global distribution of the Mercurian plains, he suggested that widespread volcanic resurfacing provides the best explanation for the origin of the intercrater plains.

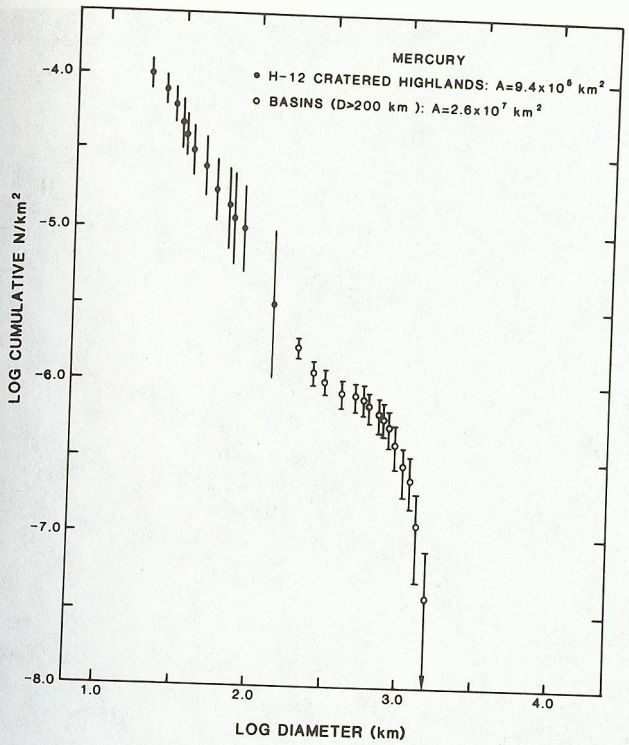

Fig. 11. Frequency-distribution of large craters and basins on Mercury. Smaller-diameter population (black dots) is a representative section of heavily-cratered terrain in the H-12 (Michelangelo) quadrangle. Larger-diameter population (open dots) includes ancient, multiring basins (Fig. 10; Table II). Bend in curve occurs between diameters of 300 and 500 km; this suggests that the intercrater plains largely obliterated a pre-existing, heavily cratered surface. Only the largest craters of this older population can be discerned.

Whatever process is invoked to explain the intercrater plains, it must be capable of explaining their global distribution and their efficacy in obliterating all craters smaller than 300 to 500 km. While no diagnostic volcanic landforms are associated with the intercrater plains, neither are there any obvious source basins to provide ballistically emplaced (Cayley-type) debris. We think that the global distribution of the intercrater plains is a compelling argument for volcanic activity being at least partly responsible for their emplacement. Because the intercrater plains were emplaced early in the planet's history, during the time of heavy impact bombardment, it is likely that these plains have been extensively brecciated and probably do not retain any remnant of original surface morphology.

In addition to ancient multiring basins and the intercrater plains, several large basins formed in the pre-Tolstojan period after most of the intercrater

Fig. 12. Intercrater plains south of Homer basin (−1°, 37°). Rough, undulating surface is due mostly to numerous superposed secondary craters. (Portion of H-6 photomosaic; north at top; width of scene 680 km.)

plains had been emplaced. These basins include Dostoevskij (see Sec. II.C and Fig. 3), Shakespeare (49°, 151°), and Homer (−2°, 38°; Fig. 12). A particularly interesting pre-Tolstojan basin is Surikov (−37°, 125°). The name was originally applied only to the peak ring of this basin. Subsequent geologic mapping (Spudis and Prosser 1984) demonstrated that Surikov is a three-ring structure, but that the outer rings are much more subdued than the innermost, peak-ring structure. This observation suggests that some type of structural rejuvenation may be partly responsible for the present morphology of Surikov

and, by extension, that such a process may be operative in the production of basin morphology elsewhere on Mercury.

B. Tolstojan System

The base of the formally named Tolstojan system is marked by the base of the distinctive lineated terrain unit composed of deposits of the Tolstoj basin impact (Fig. 2). This basal, lineated unit was named by Spudis (1985) the Goya Formation, after the unrelated pre-Tolstojan crater Goya (−7°, 152°). The Goya Formation consists of coarsely lineated to hummocky material that extends as far as one basin diameter (500 km) from the rim of the Tolstoj basin (Fig. 13). As previously discussed, the Goya Formation appears to be largely absent from the western and northwestern exterior of the basin; its total areal extent is about 7.8×10^5 km^2. The crater density on the Goya Formation serves as the reference crater density for the base of the Tolstojan system; for craters with diameter > 20 km, the reference crater density is $8.5 \pm 1.4 \times 10^{-5}$ km^{-2}. All surfaces with crater densities higher than this value are pre-Tolstojan in age.

Tolstoj displays four rings, with varying expressions of continuity and

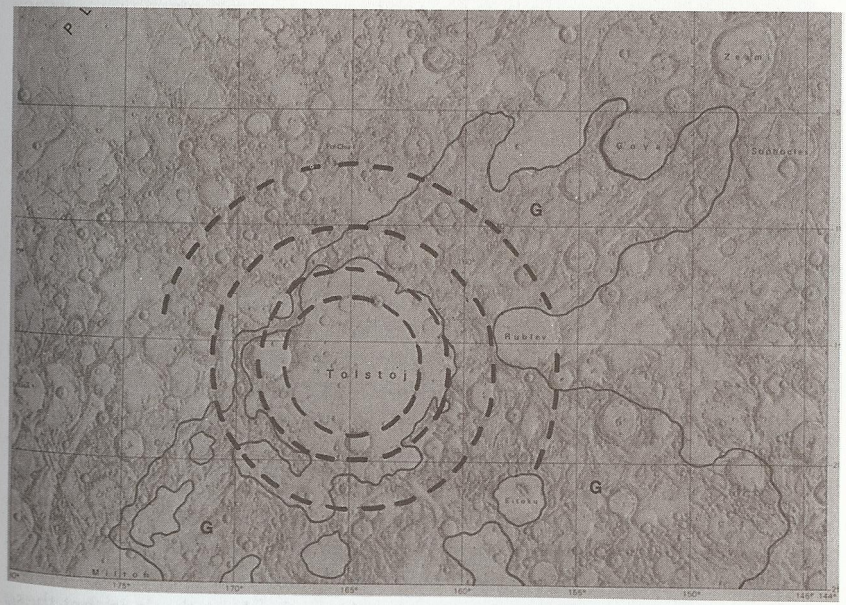

Fig. 13. Geologic sketch map of the Tolstoj basin. Tolstoj ejecta blanket (Goya Formation; G) is well exposed to northeast, southeast and south of the basin. Tolstoj displays four rings 260, 330, 510 (basin rim) and 720 km diameter (dashes). (North at top; width of scene about 1200 km.)

morphologic prominence (Fig. 13). The main basin rim consists of prominent massifs and scarps that form a ring 510 km in diameter. Other rings are more discontinuous, but may be mapped at 260, 330, and 720 km in diameter (Table II). On the floor of the Tolstoj basin are several "Archimedean" craters, i.e., craters that have formed on the basin floor before deposition of smooth plains materials in the basin interior. This stratigraphic relation and the lower crater density on the smooth plains indicates that the plains were not emplaced at the time of the Tolstoj impact, but substantially postdate the basin. Wilhelms (1976) argued that the plains fill of Tolstoj is a distal ejecta deposit of the Caloris basin; however, no Caloris basin smooth plains are observed superposed on the Goya Formation. A more likely interpretation is that the smooth plains are volcanic lavas that flooded the Tolstoj basin some time after the basin impact.

After the Tolstoj impact, numerous large craters and basins formed, including Scarlatti (40°, 100°), Durer (22°, 119°) and Renoir (−18°, 52°). All of these features are double-ring basins, which are randomly distributed around the hemisphere of Mercury imaged by Mariner 10. In addition to these small basins and craters, smooth plains materials were emplaced in late Tolstojan time, some of which are still exposed. Typically, these plains morphologically resemble the later smooth plains units, but they possess a substantially higher crater density. The Tolstojan plains generally crop out around the margins of regional deposits of younger, post-Caloris basin plains; a reasonable inference is that the present surface exposure of the older smooth plains is only a fraction of their total areal extent, the rest being buried by younger units. This observation suggests that emplacement of plains materials may have extended over most of the early history of Mercury.

The Beethoven basin (−20°, 124°) probably formed toward the end of the Tolstojan Period, based on its crater density (see Sec. II.B). Beethoven possesses a well-preserved, lineated ejecta blanket that is well exposed east and south of the basin rim (Fig. 14), but appears to be absent west of the basin. Because of the relative youth of Beethoven, this relation is probably best explained by a natural ejecta asymmetry, as in the case of Tolstoj. Beethoven displays only one ring, about 625 km in diameter; because Mariner 10 images of this basin were taken under very high Sun illumination, other rings probably exist that cannot be discerned on available images. The floor of Beethoven is covered by smooth plains that possess a considerably higher crater density than do the Caloris smooth plains (Fig. 14). These plains materials appear to have completely buried any expected interior ring of Beethoven; this implies that they are fairly thick in the basin interior. We consider it likely that these plains were formed by massive flood lava eruptions, immediately following the Beethoven impact. An alternative hypothesis is that these plains represent the original floor material of Beethoven, that an interior ring(s) never formed, and that the volume of impact melt generated by the Beethoven impact was several orders of magnitude greater than that generated

Fig. 14. Mosiac of part of the Beethoven basin (rim 625 km diameter; dashed). Basin floor is filled with older, cratered smooth plains. Lineated ejecta blanket (E) extends outward up to one basin diameter southeast of rim. (North at top.)

during the impact of other Mercurian basins. We consider this complex explanation less likely than flooding by lavas to form the plains.

C. Calorian System

Caloris Basin. The impact that formed the Caloris basin (Fig. 4) was a watershed event in the geologic history of Mercury. The extensive ejecta deposits of Caloris are presumed to have formed instantaneously within the Mercurian geologic record. These deposits therefore form a useful marker horizon and can be used to divide the geologic time scale in the same way that the ejecta of the Imbrium basin has been used on the Moon (Shoemaker and

Hackman 1962). The Caloris deposits were used as a stratigraphic marker by Guest and Gault (1976), Guest and O'Donnell (1977) and Leake (1982), who referred to stratigraphic units as pre- and post-Caloris.

The products of the Caloris impact have been formalized into a rock-stratigraphic Caloris Group, consisting of several formations (McCauley et al. 1981). This nomenclature was developed during the 1:5,000,000 scale geologic mapping of the Tolstoj (H-8) quadrangle (Schaber and McCauley 1980) and the adjacent Shakespeare (H-3) quadrangle[a] (Guest and Greeley 1983). The units designated as formations were essentially the morphological units recognized by Trask and Guest (1975), each of which was considered an individual rock unit. The mountain material was named the Caloris Montes Formation, the intermontane plains the Nervo Formation, the hummocky plains the Odin Formation, and the lineated plains were included in the Van Eyck Formation. In addition, clusters of secondary craters from Caloris were recognized by Schaber and McCauley (1980) and were included as a facies of the Van Eyck Formation.

All the formations of the Caloris Group are interpreted to represent deposits formed by the impact that formed the Caloris basin. These materials include basin impact melt, clastic ejecta, locally reworked material, and secondary crater material. The base of the Caloris Group defines the base of the Calorian system (Spudis 1985); its reference crater density ($D > 20$ km) is 5.8 $\pm$ 1.3 $\times$ 10^{-5} km^{-2}.

The Caloris basin (Fig. 4) has been the subject of several detailed geologic studies (Strom et al. 1975; McCauley 1977; McCauley et al. 1981) and is only briefly described here. (See Figs. 15-18 for rock-stratigraphic formations of the Caloris Group [McCauley et al. 1981].) The main basin rim is 1340 km in diameter; it consists of rugged massifs arranged into a concentric pattern (Fig. 15). The Caloris rim is here considered to be the structural equivalent of the main rings of lunar basins (e.g., Cordillera of Orientale; Apennines of Imbrium). Mantling the intermassif areas near the Caloris rim is the Nervo Formation (Fig. 15), which forms an undulating-to-smooth unit that is interpreted by McCauley et al. (1981) as fallback ejecta. Much of the Nervo Formation may consist of impact melt, ejected from the excavation cavity of the basin; it resembles small melt ponds observed in the ejecta of the lunar Orientale basin. The Odin Formation (Fig. 16) consists of knobby, plains-like deposits that are widely exposed directly east of the basin rim. The Odin Formation morphologically resembles knobby basin deposits found around lunar basins, such as the Alpes Formation of the Imbrium basin (McCauley et al. 1981). Large tracts of the Odin Formation apparently are partly buried by later smooth plains materials (Fig. 16).

[a]In the Shakespeare quadrangle map (Guest and Greeley 1983), the Odin Formation—mantling deposit (com) and the Van Eyck Formation (cvl) have been wrongly labeled in the description of units, although they are correctly designated in the accompanying text.

Fig. 15. Caloris Montes Formation (M), forming the southern rim of the Caloris basin. Nervo Formation (N) occurs between massifs. Lineated facies of Van Eyck Formation (VEL) at lower right (FDS 111). (North at top.)

Fig. 16. Knobby deposits of the Odin Formation (O). Caloris deposits are partly mantled in this region by smooth plains (P) (FDS 73). (North at top.)

The radially lineated ejecta blanket of the Caloris basin is expressed by the Van Eyck Formation, lineated facies (see Figs. 15 and 17). This unit is equivalent to the lunar Fra Mauro Formation of the Imbrium basin. The Van Eyck Formation, lineated facies, is not widely exposed around the Caloris basin, and apparently was largely buried by subsequent smooth plains materials (Fig. 15). The other facies of the Van Eyck Formation, secondary craters, is well exposed in the highlands southeast of Tir Planitia (Fig. 18). Caloris basin secondary craters consist of groups or chains of large (10–20 km), overlapping, irregular craters. No recognizable Caloris secondaries have been found on the smooth plains surrounding the basin, indicating that the plains postdate all recognized basin secondaries.

An unusual terrain, consisting of hilly and furrowed material, occurs near the antipode of the Caloris basin around −25°, 20°. Schultz and Gault (1975) and Hughes et al. (1977) have provided compelling arguments that this terrain was produced by the global focusing of seismic waves associated with the Caloris impact. Although these materials are not a member of the Caloris Group (McCauley et al. 1981), we accept the interpretation of their origin by Caloris basin seismic waves, and we therefore assume that these hilly and furrowed units on the opposite side of Mercury from Caloris demarcate the base of the Calorian System in their region of occurrence.

Fig. 17. Nervo Formation (N) and lineated facies of Van Eyck Formation (VEL). The large crater is Nervo, 50 km in diameter (FDS 103). (North at top.)

Fig. 18. Secondary crater facies of Van Eyck Formation (arrows) (Portion of H-8 photomosaic; north at top.)

The ring system of the Caloris basin has been the subject of some controversy. The only obvious ring is the 1340 km main basin rim, defined by the Caloris Montes Formation. However, the Caloris basin is centered within a broad, regional concentric pattern that is formed by wrinkle ridges, scarps and physiographic boundaries, both inside and outside the Caloris basin (Fig. 19a). The smooth plains/highlands contact in the H-8 quadrangle forms a major physiographic boundary concentric with the Caloris basin, and some major dorsa (e.g., Schiaparelli dorsum) are also concentric with the basin rim. Experience with the geologic mapping of the lunar basins (e.g. Imbrium; see Spudis 1986) suggests that regional mapping of concentric structures can aid

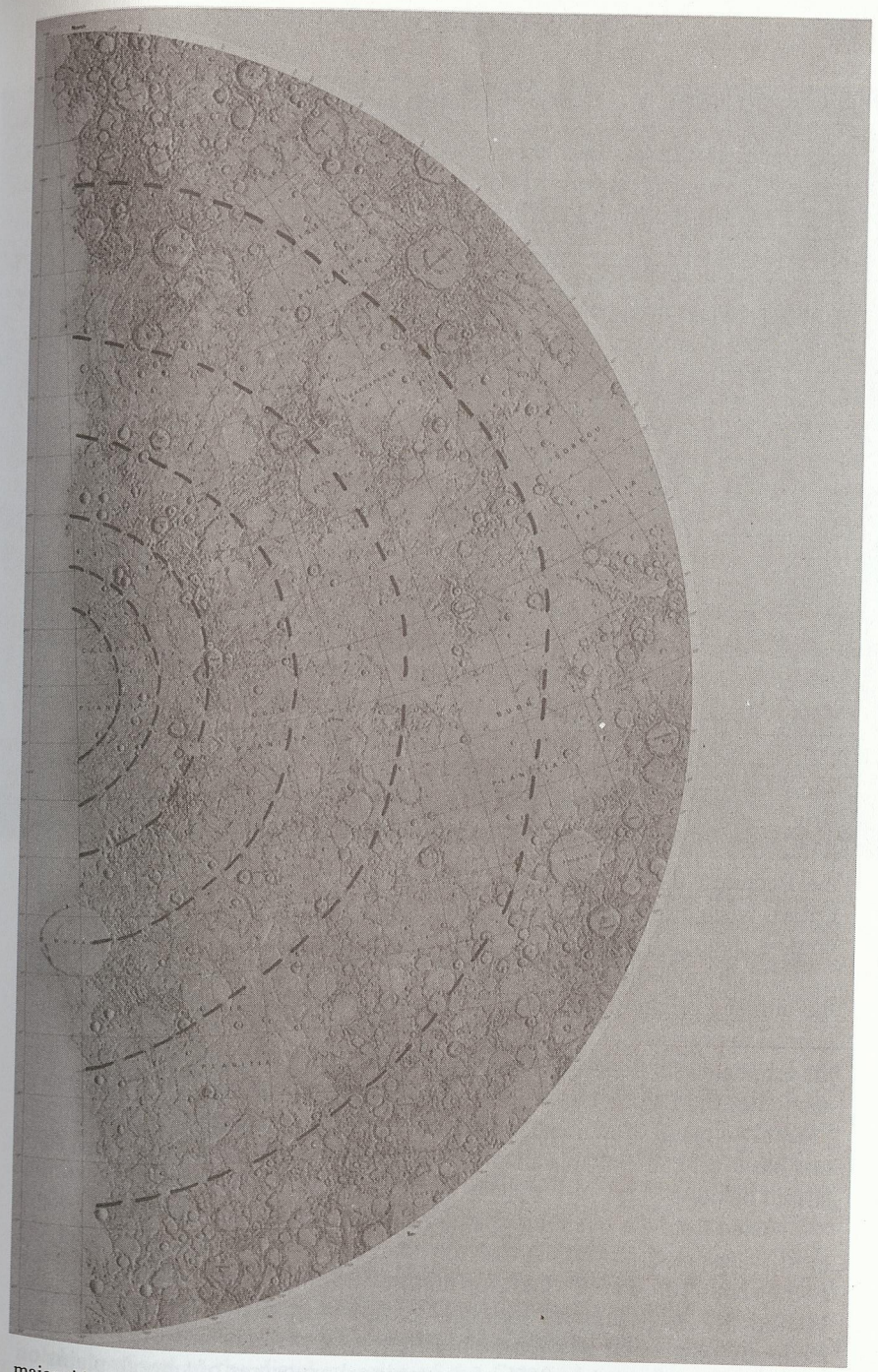

Fig. 19. Basin-centered view of Caloris basin showing distribution of basin radial and concentric structures. Stereographic projection by U.S. Geological Survey. (North at top.) (a) Map of major ridges within Caloris Planitia and smooth plains exterior to Caloris basin, and (b) Ring interpretation map, based on (a). See Table II for ring diameters.

in the delineation of subdued basin rings. On this principle, we present a regional map of structures around the Caloris basin (Fig. 19a) and a ring interpretation map based on these features (Fig. 19b). In this reconstruction, Caloris displays six rings, ranging from 630 km to 3700 km in diameter (Fig. 19b; Table II). Caloris bears a striking similarity to the lunar Imbrium basin, also a six-ring basin, containing two rings interior and three rings exterior to the main basin rim (Schultz and Spudis 1985; Spudis 1986); both basins are of similar size and morphology. In addition, both Imbrium and Caloris display large tracts of smooth plains in a broad, exterior arc external to the basin rim (Oceanus Procellarum around Imbrium; Tir, Odin and Susei Planitia around Caloris).

The striking parallels between the lunar Imbrium and Mercurian Caloris basins indicate that a similar sequence of events was responsible for the development of both. This similarity, in addition to other relations of the Mercurian smooth plains discussed below, suggests that the bulk of the smooth plains of Mercury are of volcanic origin and are related to the Caloris basin impact only in the same sense that the lunar maria are related to their containing basins, i.e., as younger geologic units deposited in structural and topographic lows.

Calorian plains materials. In the above discussion on the Caloris Group, the floor material of the Caloris basin (see Figs. 4 and 20) was specifically excluded. McCauley et al. (1981) considered that this material was of uncertain relevance to the basin. The Caloris floor material displays numerous wrinkle ridges (indicative of surface compression) and graben-like troughs (indicative of surface tension; Fig. 20). The wrinkle ridges are cut by (predate) the fractures; the implication of these observations is that the floor of the Caloris basin originally subsided, and then uplifted, possibly as a result of updoming (rebound) in the basin interior (Strom et al. 1975; Dzurisin 1978).

This hypothesis for the history of the Caloris basin floor does not address the ultimate origin of the basin floor plains. We suggest, on the basis of the general appearance of undeformed portions of the basin floor (Fig. 20), that the original basin floor of Caloris was flooded by smooth plains volcanic lavas soon after the Caloris impact; the subsequent deformation described above is probably a result of regional, postbasin tectonic activity. The age of the Caloris basin-fill material appears to be slightly younger than Caloris ejecta (discussed below).

Aside from the intercrater plains, the Calorian-age smooth plains are the most widespread plains materials on Mercury (Fig. 21); the smooth plains cover about 10.4×10^6 km^2, or almost 40% of the total area imaged by Mariner 10. In contrast to some earlier opinions, the Calorian-age smooth plains are distributed all over the hemisphere of Mercury imaged by Mariner 10. Moreover, more than 90% of the regional exposures of smooth plains on Mercury are associated with basin depositional environments (cf. Figs. 10, 19b and 21). Smooth plains also occur as fill materials for both smaller double-ring basins and large craters.

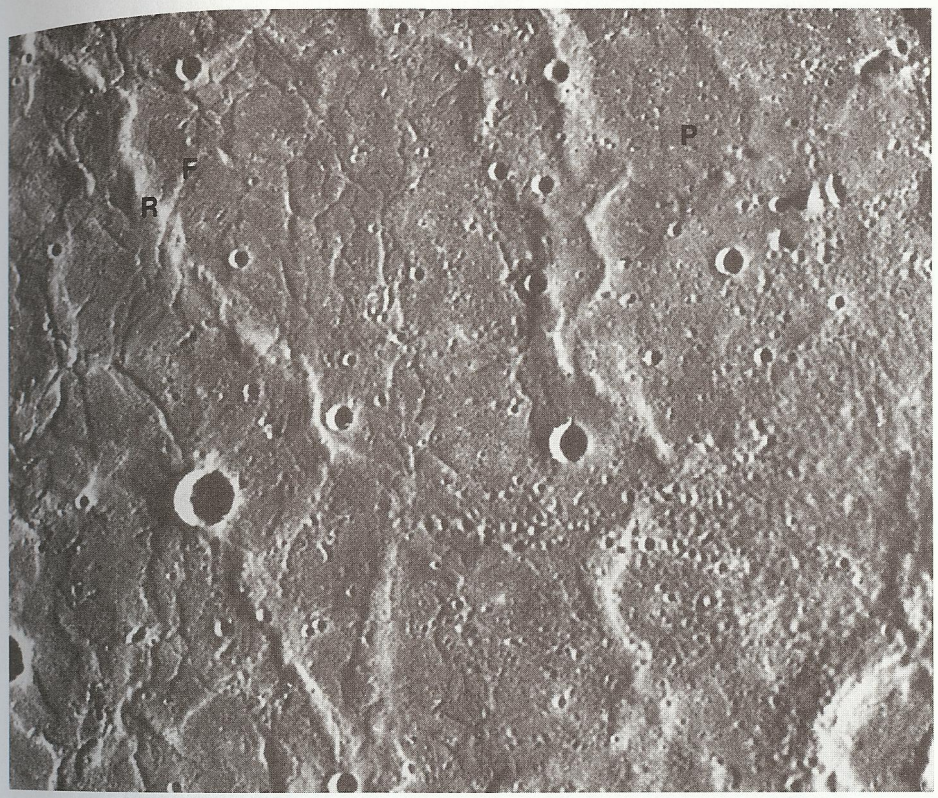

Fig. 20. Caloris basin floor materials. Wrinkle ridges (R) are cut by fractures (F). Portions of floor appear similar to smooth plains (P), suggesting that Caloris basin fill consists of smooth plains material, tectonically deformed (FDS 106). (North at top; width of scene 250 km.)

For the purpose of this study, we have made new crater counts for a variety of Mercurian geologic units (Table III). Results indicate that both the Caloris basin floor material and the smooth plains exterior to and concentric with the Caloris basin are younger than the basin ejecta. These data support the geological arguments in the previous section that the Mercurian smooth plains are not genetically related to Caloris basin ejecta, but were emplaced (apparently within a limited time) well after the Caloris impact.

In the debate regarding the origin of Mercury's smooth plains, several geological constraints may now be placed on the generating mechanism. First, the smooth plains have a planetwide distribution (Fig. 21), and are not solely confined to the distal margins of the Caloris basin. Second, the total volume of the smooth plains, whose estimation must now be greatly increased over the large estimates of Strom et al. (1975) and Trask and Strom (1976), is much greater than that which could be reasonably expected from the Caloris

TABLE III
Crater Densities for Some Mercurian Geologic Units.

Unit	Region[a]	Area (10^3 km^2)	Number ($D \geq 20$ km)	Density (10^{-5} km^{-2})[b]
Smooth plains	H-3	494	12	2.4 ± 0.7
Smooth plains	H-8	528	15	2.8 ± 0.7
Smooth plains	H-3; H-8	1022	27	2.6 ± 0.5
Caloris floor	H-3	280	11	3.9 ± 1.2
Bach basin	H-12	120	5	4.2 ± 1.9
Caloris basin	H-3	360	21	5.8 ± 1.3
Beethoven basin	H-7; H-12	440	31	7.0 ± 1.3
Tolstoj basin	H-8	413	35	8.5 ± 1.4
Dostoevskij basin	H-12	360	45	12.5 ± 1.9
Surikov basin	H-12	120	19	15.8 ± 3.6

[a]Region refers to USGS quadrangle maps where crater counts were done.
[b]Crater density plus one standard deviation.

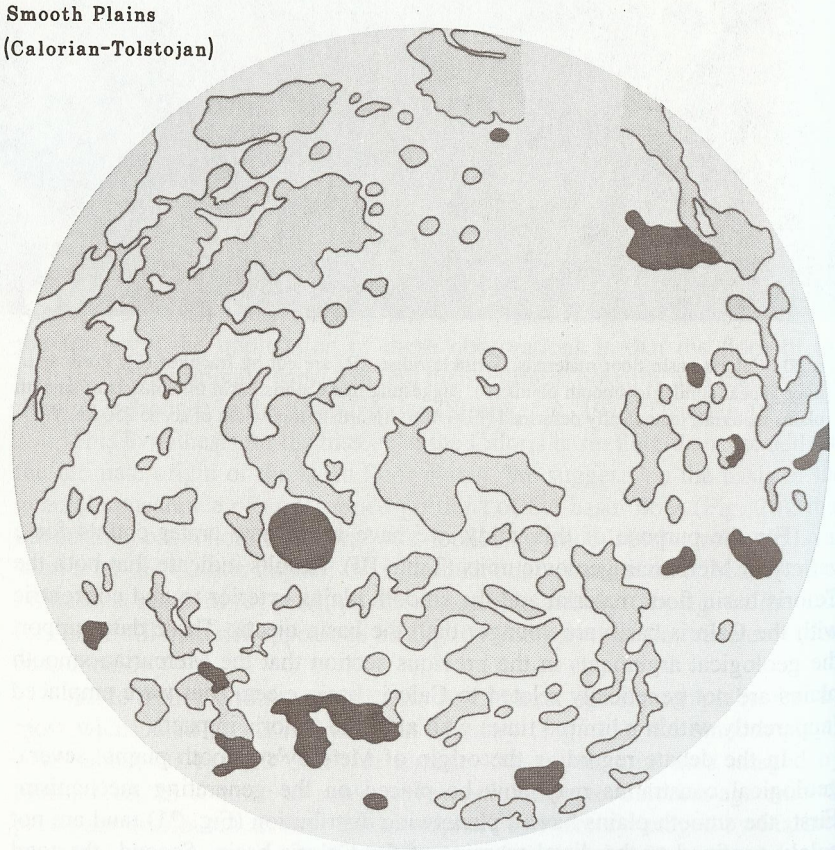

Fig. 21. Distribution of Calorian (light grey) and Calorian and/or Tolstojan (dark grey) smooth plains. Smooth plains cover about 10.4×10^6 km^2 or 40% of the part of Mercury photographed by Mariner 10. Base is a Lambert equal-area projection, centered on 0°, 100°. (North at top.)

impact, or several Caloris-sized impacts. Third, crater-density data (Table III) indicate that major expanses of the circum-Caloris smooth plains substantially postdate all recognized major Mercurian basins.

By analogy with the lunar maria, these constraints support the hypothesis that the Mercurian smooth plains were emplaced as volcanic lavas, created during partial melting of Mercury's mantle. The long-standing reluctance on the part of some investigators to accept the volcanic hypothesis for smooth plains emplacement appears to be motivated partly by the lack of diagnostic volcanic morphologies in the smooth plains and partly by the lack of any color or albedo contrast between the plains and the cratered terrain on Mercury. Schultz (1977) and Malin (1978) have pointed out that the apparent absence of volcanic landforms is largely due to the poor coverage and resolution of Mariner 10 data; similar coverage of the Moon would likewise reveal few, if any, volcanic features in the lunar maria. The lack of albedo contrast between Mercurian plains and cratered terrain may simply reflect a generally lower FeO, and possibly TiO_2, content of Mercurian vs lunar lavas (Hapke et al. 1975; Strom 1984). The typical albedo of the circum-Caloris smooth plains is about 0.12 to 0.13 (Hapke et al. 1975). This value is identical to that of a regional light plains deposit on the Moon, the Apennine Bench Formation. Geologic and remote-sensing studies have shown that these lunar plains are probably composed of extrusive basaltic rocks (Spudis and Hawke 1986) that are higher in Al_2O_3 and lower in FeO than typical lunar mare basalts. Thus, the lack of an albedo contrast between the Mercurian smooth plains and highlands does not necessarily support an impact-ejecta origin for the plains.

Although these arguments are indirect, we consider that the evidence for a volcanic origin for the Mercurian smooth plains is compelling; similar conclusions were reached by Kiefer and Murray (1987). The age and distribution of the smooth plains suggest that Mercury underwent large-scale volcanic resurfacing after the Caloris basin impact.

Tectonic features. The tectonic features and history of Mercury are discussed in detail elsewhere in this book (see the chapter by Melosh and McKinnon) and will not be dealt with directly here. However, the lobate scarps of Mercury are of great importance to the geologic evolution of the planet, and stratigraphy can place some constraints on their time of formation.

The lobate scarps are widely distributed over Mercury (Strom et al. 1975). They consist of sinuous to arcuate scarps that transect pre-existing plains and craters (Fig. 22). They are most convincingly interpreted as thrust faults, indicating a period of global compression (Strom et al. 1975; Solomon 1977). All these scarps cut intercrater plains materials, which suggests that they began to form after the intercrater plains materials were emplaced in pre-Tolstojan time. Additionally, Dostoevskij basin ejecta (Fig. 3) is cut by a lobate scarp, Hero Rupes; this suggests that scarp formation began some time in the late pre-Tolstojan period. The lobate scarps typically transect smooth

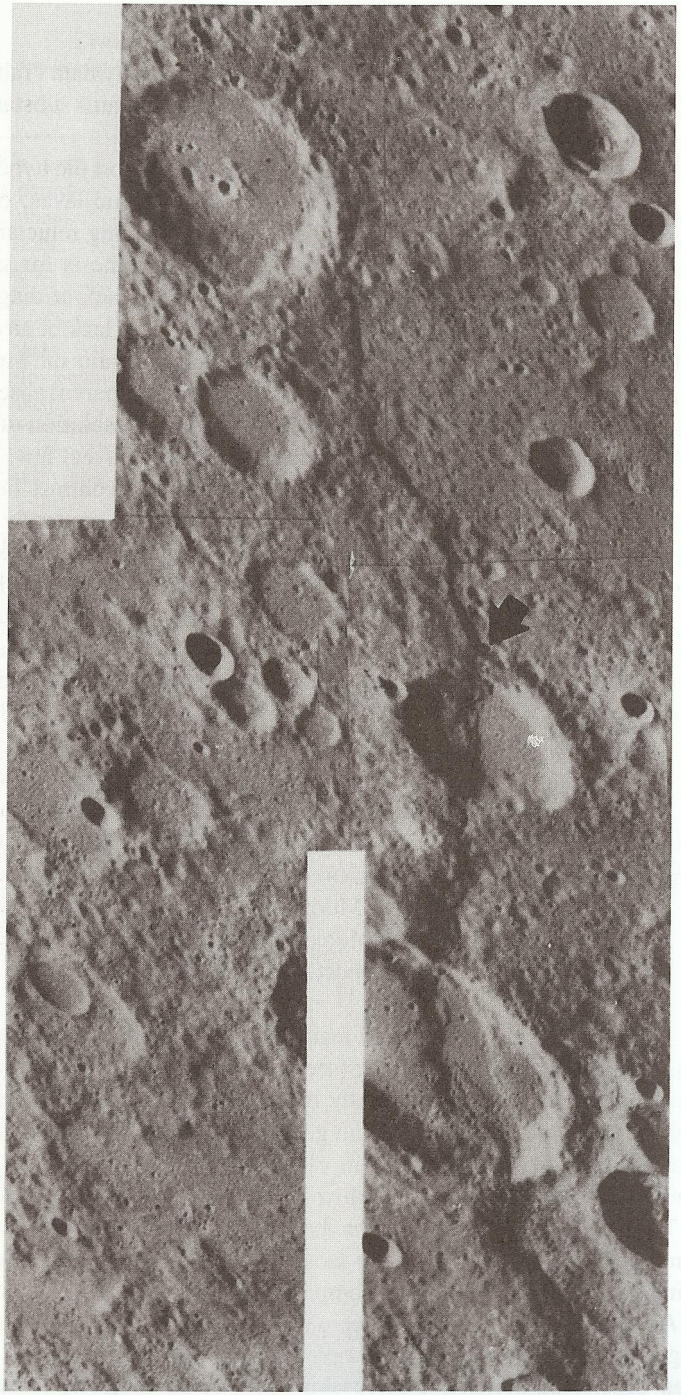

Fig. 22. View of Discovery Rupes, one of a global system of lobate scarps. Crater offset (arrow) suggests these scarps are thrust faults. (North at top; portion of H-11 photomosaic.)

plains materials (early Calorian age) on the floors of craters (Fig. 22). Strom (1984) notes that superposed craters are of the Class 1 and 2 degradational types (Kuiperian and Mansurian age). These observations suggest that lobate-scarp formation was confined to an interval beginning roughly in the late pre-Tolstojan Period and ending in the middle to late Calorian Period.

In addition to the lobate scarps, numerous wrinkle ridges occur in the smooth plains materials (see Figs. 4 and 20). These ridges probably were formed by local to regional surface compression caused by lithospheric loading by dense stacks of volcanic lavas, as suggested for those of the lunar maria (Solomon and Head 1980).

Calorian craters and basins. Although Caloris was the last major basin-forming impact on Mercury, numerous smaller two-ring basins formed during the Calorian Period and are randomly distributed over the planet. Such basins include Strindberg (53°, 136°), Rodin (21°, 18°), Michelangelo (−35°, 109°) and Bach (−69°, 101°; Fig. 23). These two-ring basins are well preserved, display in most cases an exceptionally complete peak ring, and are commonly filled with smooth plains materials. In addition to these small basins, numerous craters of Calorian age are widely distributed over the planet. Many of these craters are partly to completely flooded by smooth plains materials.

D. Mansurian System

The Calorian Period witnessed what was virtually the last major, regional cycles of geologic activity on Mercury. After the final deposition of smooth plains materials, only impact craters have formed on the Mercurian surface. Rocks formed in the long interval of time between the smooth plains emplacement and the present are divided into two chronostratigraphic systems. The lower contact of deposits from the crater Mansur (48°, 163°), shown in Fig. 24, defines the base of the Mansurian System. This system, like the lunar Eratosthenian System (Table I), includes materials of slightly degraded, but still relatively fresh craters, some of which contain minor plains materials. All of these Mansurian-age plains are confined to crater floors and they most likely consist of crater impact-melt sheets and fallback ejecta deposits. Mansurian-age craters possess no rays, but fine-scale structures in their ejecta deposits are largely preserved (Fig. 24). All craters of this age are randomly distributed over the planet and no regional deposits of plains of Mansurian age have been recognized.

E. Kuiperian System

The end of the Mansurian system is loosely defined by superposed, rayed craters, typified by the deposits of the crater Kuiper (−11°, 31°.5) shown in

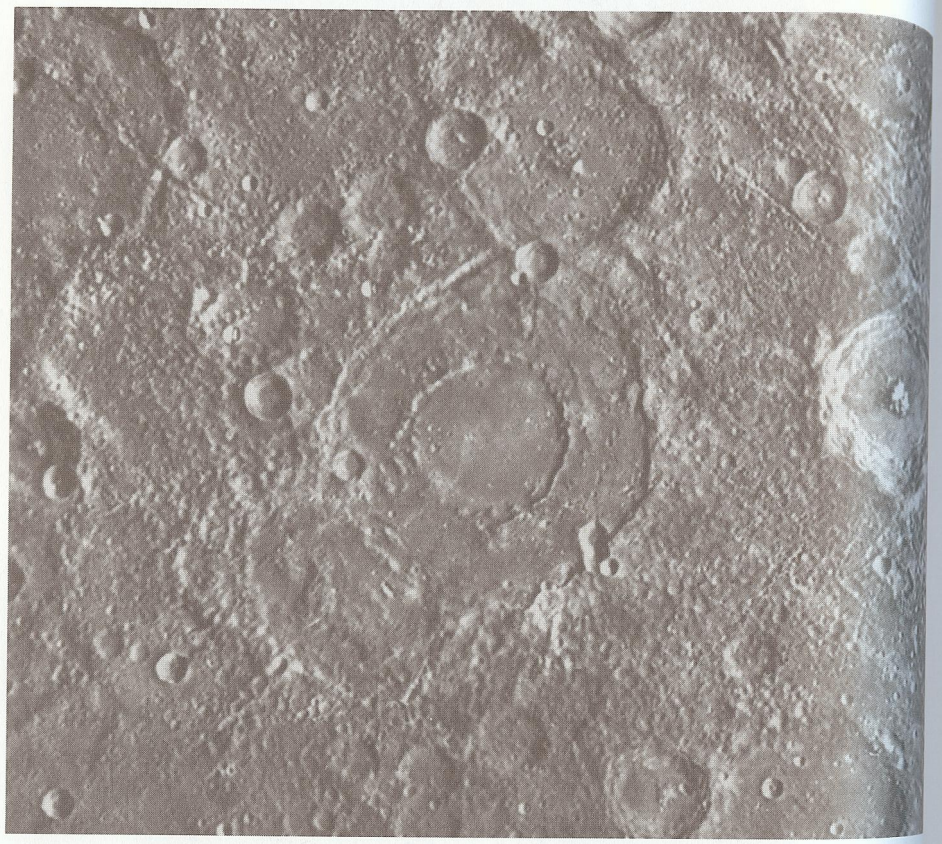

Fig. 23. Calorian age two-ring basin Bach (−69°, 101°; 210 km diameter). Inner peak ring (103 km diameter) is exceptionally well preserved and basin is flooded by younger smooth plains materials. (North at top; portion of H-15 photomosaic.)

Fig. 25. The Kuiperian System includes the formation of all fresh, rayed craters on Mercury, extending to the present; it is composed wholly of crater deposits, almost all, of which are only slightly degraded if at all and still possess bright ray systems (Fig. 25). This system is thus analogous to the lunar Copernican System (Table I). Several unusual high-albedo markings with swirl-like appearance have been recognized near the crater Handel (4°, 34°) by Schultz and Srnka (1980); they suggested these swirls are geologically young (thus Kuiperian in age) and were produced during the impact of a cometary coma by scouring the Mercurian surface with hot gases and high-energy plasmas. Other than this unusual feature, no regional deposits of Kuiperian age have been recognized.

Fig. 24. Mansur crater (48°, 163°; 75 km diameter). The base of deposits from this crater define the top of the Calorian and bottom of the Mansurian Systems. (North at top; portion of H-3 photomosaic.)

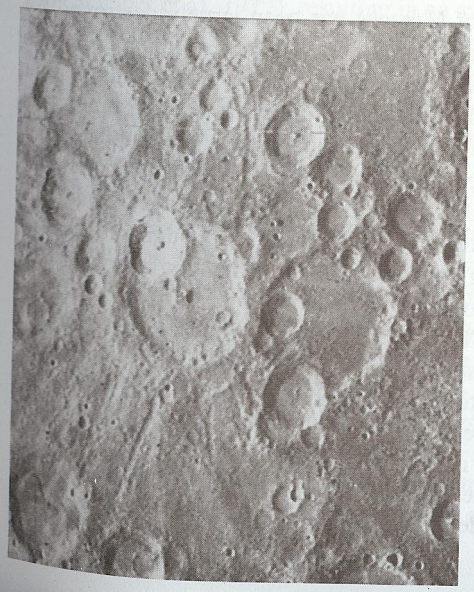

Fig. 25. Kuiper crater (−11°, 31°5; 60 km diameter). The base of deposits from this crater define the top of the Mansurian and bottom of the Kuiperian Systems (FDS 27304) (North at top.)

IV. GEOLOGIC HISTORY OF MERCURY

The chronostratigraphic scheme described above has been used to make a global geologic map of Mercury at a scale of 1:10,000,000 (Spudis in preparation). We have used this geologic map to prepare a series of paleogeologic maps, showing our best estimate of the changing appearance of Mercury through time (see Plates 1-6 in the color section). The five maps show the distribution of geologic units in middle pre-Tolstojan (Plate 2), early Tolstojan (Plate 3), early Calorian (Plate 4), middle to late Calorian (Plate 5), and Kuiperian times (Plate 6). The last map (Plate 6) shows the current surface geology of Mercury and is an abstract of the new global map at 1:10,000,000 scale.

A. Summary of Mercury's Geologic Evolution

The earliest decipherable geologic event in Mercury's history was the formation of its crust. On the basis of analogy with lunar history, Warren (1985) considers that Mercury underwent early global crustal melting. This process, called the "magmasphere" stage by Warren (1985), would have been similar to the lunar "magma ocean", whereby large-scale melting of at least the outer few hundred kilometers of the planet would tend to concentrate low-density plagioclase feldspar into the uppermost part of the Mercurian crust. If this process operated during Mercury's early history, its crust is composed largely of anorthositic rocks (anorthosites, anorthositic norites and anorthositic gabbros). This is consistent with the limited full-disk spectra of Mercury obtained by McCord and Clark (1979), which suggest that Mercury's surface is compositionally similar to Apollo 16 highland soils. However, these data are of such limited quality that few constraints can be placed on Mercury's surface composition.

The earliest cratering record of Mercury has been largely destroyed by the deposition of the intercrater plains. However, the largest impact features of this period (multiring basins) have been partly preserved and suggest that Mercury's surface may have originally resembled the cratered lunar highlands (Color Plate 2). Sometime during the heavy bombardment, the emplacement of massive quantities of intercrater plains materials largely obliterated the older crater population. The global distribution of the intercrater plains suggests that they may be at least partly volcanic in origin, although subsequent cratering probably reduced the original surface to breccia and primary surface morphologies were probably destroyed.

The impact that formed the Tolstoj basin marked the beginning of the Tolstojan Period (Color Plate 3), still a time of high impact rates. Although some flood lavas may have erupted during this time, their preservation is sporadic (Fig. 14) and they may be largely covered by subsequent lavas. The Beethoven basin probably formed near the end of the Tolstojan Period.

The Caloris impact formed the largest well-preserved basin on Mercury's surface (Color Plate 4) and provided an extensive stratigraphic datum on the

planet. Catastrophic seismic vibrations from the Caloris impact probably formed the hilly and furrowed terrain on the opposite side of the planet. Some finite, but probably short, time after the Caloris impact, came massive extrusions of flood lavas to form the Mercurian smooth plains (Color Plate 5). A rapidly declining cratering rate has produced minimal changes to Mercury's surface (Color Plate 6) since the final emplacement of the smooth plains. This low cratering rate presently continues to produce regolith on all Mercurian surface units.

B. Interplanetary Comparisons

The chronostratigraphic systems used in the geologic mapping of Mercury are similar to those used for the Moon (Table I). On both bodies, almost all geologic activity occurred early in planetary history—during pre-Tolstojan to early Calorian time on Mercury and pre-Nectarian to early Imbrian time on the Moon (Wilhelms 1984;1987*a*). A significant difference between the two planets is the continued period of mare deposition on the Moon, which may have continued into Copernican time (Schultz and Spudis 1983). Such a wide range in age for plains material is not evident on Mercury, at least within the hemisphere imaged by Mariner 10.

Previous studies of the Mercurian basin population have emphasized the apparent deficiency of basins on Mercury relative to the Moon (Malin 1976*b*; Schaber et al. 1977; Frey and Lowry 1979). Wood and Head (1976) considered that Mercury has a high basin density, but they included many complex craters and protobasins in their sample; the first 19 entries in their table of Mercurian basins are all smaller than 200 km in diameter. The cumulative basin density on Mercury ($D \geq 200$ km) is reported by Schaber et al. (1977) to be only 37% of that on the Moon. The Moon has at least 62 basins, $D \geq 200$ km (Schaber et al. 1977), resulting in an average basin density of $1.72 \pm 0.13 \times 10^{-6}$ km^{-2}. Only about 35% of Mercury's surface was photographed by Mariner 10 with lighting conditions adequate (Strom 1979) to recognize ancient basin structures. The degraded basins recognized by systematic geologic mapping (Sec. III.A; Table II) suggest that Mercury has at least 50 two-ring and multiring basins ($D \geq 200$ km) within this area. Thus, the average density of Mercurian basins is $1.92 \pm 0.14 \times 10^{-6}$ km^{-2}. This value suggests that Mercury is not deficient in multiring basins and may possibly have more per unit area than the Moon. The presence of a large population of basins that predate the Mercurian intercrater plains suggests that basin production was a continuous process during the early history of the planets.

The relative ages of some comparable Mercurian and lunar geologic units may be plotted against crater densities to estimate the cratering rates in the early histories of the two planets (Fig. 26). Although we have radiometric ages for only a few lunar geologic units (Fig. 26b), it is clear that the general shapes of the two curves may be interpreted to be similar. Deposition of the smooth plains materials on Mercury was essentially that planet's last global

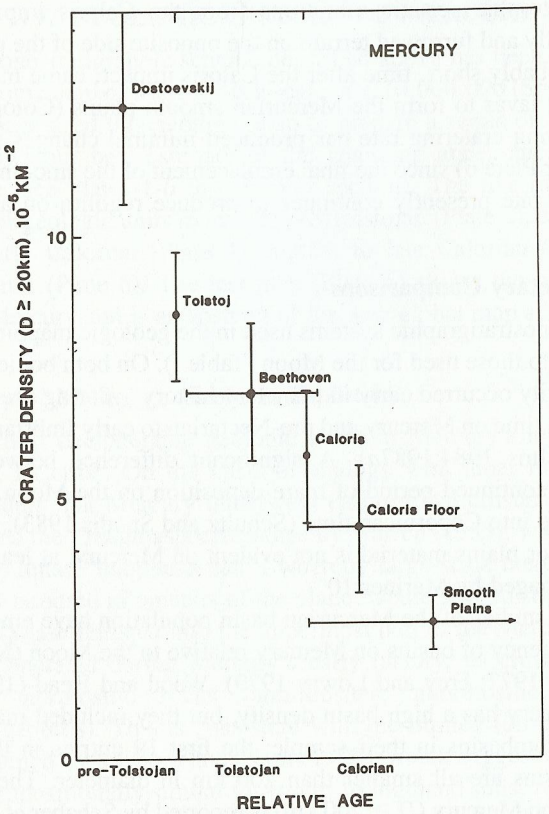

Fig. 26. Plots of crater density on various geological units on Mercury and the Moon versus stratigraphically defined relative ages. *Mercury*: Tolstoj and Caloris have no horizontal error bars because they define beginning of stratigraphic systems. Note that both Caloris basin fill and exterior smooth plains postdate Caloris basin ejecta. See Table III. *Moon*: Nectaris and Imbrium have no horizontal error bars because they define beginning of stratigraphic systems. Crater densities for lunar basins from Wilhelms (1987*a*); data for average maria from Basaltic Volcanism Study Project (1981). Note that for comparable stratigraphic positions, the lunar units display somewhat lower absolute crater densities than Mercurian units. Absolute ages in billion (10^9) years.

geologic event and only impact craters have formed since then. Crater densities on the Mercurian smooth plains are comparable to the crater density on the lunar Imbrium basin deposits (Fig. 26; see also Murray et al. 1974). This may imply that the last major geologic activity occurred on Mercury roughly 3.8 Gyr ago (Basaltic Volcanism Study Project 1981), although it is by no means certain that absolute ages may be directly compared between the two bodies (Chapman 1976). In any event, it appears that Mercury, like the Moon, was most active geologically early in its history although the comparative

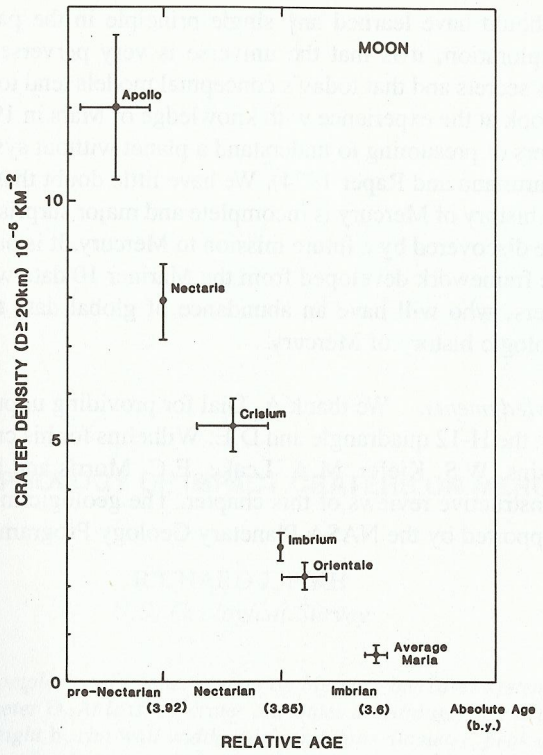

timing of the decline in impact-cratering rate and somewhat later cessation of volcanism must await radiometric dating of samples collected from the surface. Whatever the timing, no relatively uncratered units, such as are widespread on Mars (Scott and Carr 1978; Basaltic Volcanism Study Project 1981), so far have been observed. Thus, there has been no extensive resurfacing of Mercury in its more recent history. The question remains, however, why the Moon and Mercury, with such different internal structures, had such apparently similar surface histories.

V. CONCLUSION

The preceding discussion on the geologic evolution of Mercury is based entirely on the data returned more than a decade ago by the Mariner 10 mission. Roughly 40% of the surface of the planet has been examined at resolutions comparable to that of Earth-based telescopic observations of the Moon. Our knowledge of Mercury is similar to our knowledge of the Moon in about 1965, after the first three Ranger missions. We now perceive that Mercury is a planet that underwent intensive, early impact bombardment and widespread resurfacing by volcanic lavas, which essentially ended as much as 3 Gyr ago.

If we should have learned any single principle in the past 25 years of planetary exploration, it is that the universe is very perverse about rapidly disclosing its secrets and that today's conceptual models tend to be naive. One only has to look at the experience with knowledge of Mars in 1970 to appreciate the dangers of presuming to understand a planet without systematic global mapping (Hartmann and Raper 1974). We have little doubt that our model for the geologic history of Mercury is incomplete and major surprises may well be waiting to be discovered by a future mission to Mercury. It is our hope that the stratigraphic framework developed from the Mariner 10 data will be useful to future workers, who will have an abundance of global data to decipher the complex geologic history of Mercury.

Acknowledgments. We thank A. Dial for providing unpublished crater-count data in the H-12 quadrangle and D.E. Wilhelms for his crater-count data on lunar basins. W.S. Kiefer, M.A. Leake, E.C. Morris and D.E. Wilhelms provided constructive reviews of this chapter. The geologic mapping of Mercury was supported by the NASA Planetary Geology Program.

GEOMORPHOLOGY OF IMPACT CRATERS ON MERCURY

RICHARD J. PIKE
U.S. Geological Survey

Morphologic complexity of impact craters on Mercury increases systematically with their diameter D. *At least 15 crater attributes are strongly size dependent: depth* d, *rim height* h, *rim-wall width, peak and floor diameter, peak and rim-wall complexity, ring frequency and spacing, and presence/absence of a bowl-shaped interior, central peak, flat floor, scalloped rim crest, slump deposits, and rim-wall terraces. The 447 crater sample divides into 7 groups that resemble lunar classes, although size ranges are more like those on Mars: simple (0.225 km* ≤ D ≤ *14.4 km), modified-simple (4.6 km* ≤ D ≤ *12.2 km), immature-complex (9.5 km* ≤ D ≤ *29.1 km), and mature-complex (30.0 km* ≤ D ≤ *160 km) craters, protobasins (72 km* ≤ D ≤ *165 km), two-ring basins (132 km* ≤ D ≤ *310 km), and multiring basins (285 km* ≤ D ≤ *1600 km). Linear log-log regressions of* d *on* D *for simple* (n = *104) and complex* (n = *127) craters resolve ambiguities in past Mercurian* d/D. *The equations intersect at* D = *4.7* ± *0.6 km, half the previous value. Terrain-related contrasts in* d/D *exist only for modified-simple craters, which are shallower on smooth plains. Comparable* D *from* d/D *fits for the Earth, Mars and the Moon [1.9, 3.1, and 8.6 (mare) and 10.9 km (upland)] all differ. Linear fits to* h/D *on Mercury intersect at* D = *11 km, less than the old value (16 km) and, importantly, much more than the diameter of the inflection in* d/D. *The diameter of the transition from simple to complex craters,* D_t, *on Mercury is 10.3* ± *4 km, much less than the 16 km determined from prior work. It was recalculated from new morphologic observations and* d/D *and* h/D *data* (n = *10). The new* D_t *and comparable values for the Earth, Mars and the Moon (3.1, 5.8, and 19 km) scale strongly (inversely) with surface gravity* g *and even more so with* g *and the approach velocity of asteroids and short-period comets* g/V_∞. *Thus, Mercurian and lunar craters differ significantly in size dependence of form. Mercury's protobasins, large craters with both a central peak and an inner ring, differ significantly from two-ring basins as well as from craters: (1) both interior features in protobasins are propor-*